A PHYSICALLY-MOTIVATED TRIODE MODEL FOR CIRCUIT SIMULATIONS

Kristjan Dempwolf and Udo Zölzer

Dept. of Signal Processing and Communications,
Helmut Schmidt University Hamburg
Hamburg, Germany
kristjan.dempwolf@hsuhh.de

ABSTRACT

A new model for triodes of type 12AX7 is presented, featuring simple and continuously differentiable equations. The description is physically-motivated and enables a good replication of the grid current. Free parameters in the equations are fitted to reference data originated from measurements of practical triodes. It is shown, that the equations are able to characterize the properties of real tubes in good accordance. Results of the model itself and when embedded in an amplifier simulation are presented and align well.

1. INTRODUCTION

The theory of vacuum tubes was already discussed at full length many decades ago and the best books on these devices were still written in the 1930s to 1950s [1, 2, 3, 4]. The idea of modeling tubes intends not to challenge the correctness of the traditional formulations that can be found in those books. It is more the task of emulating the behavior of tubes at their boundaries of purpose. While the first tube models were inspired by the desire for SPICE-based simulations of hi-fi circuits, the newer approaches are rather motivated by real-time simulations and guitar amplifier circuits. These amplifier designs gain their special sound by intentionally provoking a distortion of the instruments' signal and thus have just a little in common with ordinary amplifier theory. The recent activities towards tube modeling consider the operation in overdriven amplifiers [5].

With the digital simulation of analog audio circuits in mind, the investigation of tube models is a natural next step. Any improvement in the critical parts promises better performance of the complete simulation. Such improvements include challenges such as accuracy, computational complexity and robustness.

The paper is organized as follows: The second section will review the physical fundamentals of vacuum tubes. This is necessary, because for a successful modeling of tubes or tube circuits, a good knowledge of the theory is required. The tube experts may skip this part. In Section 3 practical tubes are discussed. After this some modeling approaches are reviewed in Section 4 and the new contribution is introduced in Section 5. Finally, in Section 6, some results are presented, utilizing the model equations in the state-space model of a common amplifier stage.

2. VACUUM TUBE BASICS

In this section we give a very brief introduction to the fundamentals of vacuum tubes. For detailed exploration we refer to the historic standard literature [1, 2, 3, 4]. Because of a certain contribution to our triode model, we start with a view to simple vacuum diodes.

2.1. Diode Characteristics

The most simple vacuum tube, the so-called vacuum diode, consists of only two electrodes which are mounted in a vacuum cylinder. One electrode, the *cathode* (K), is heated and hence electrons are emitted. The second electrode is called the *anode* or *plate* (A) and is designed to collect the emitted electrons. Since electrons can not be emitted by the cold anode the assumption of unilateral conductivity is valid. In unheated condition, no current flow is possible.

2.1.1. Initial Velocity Current

Without an external voltage applied to the anode, and even for a slightly negative anode with respect to the cathode, some of the faster electrons reach the anode and a small current flow is observed. A small negative voltage must be applied in order to suppress the current flow. The current through the diode I follows the exponential equation

$$I = I_0 \cdot e^{\frac{V}{E_T}}, \tag{1}$$

with anode voltage V, thermal voltage E_T (in Volt) and current I_0 at zero voltage.

2.1.2. Space-Charge Current

When a positive voltage is applied from anode to cathode, the emitted electrons are pulled by the anode and an increasing current flow is observed. But only a part of the emitted electrons reach the anode. Most of them have only low velocity, they stay near the hot cathode and form the *space charge*, a cloud of negative charges. The resulting current depends on the anode voltage and is self-limited by reason of the electric field of the (negative) charges. This is expressed by the Langmuir-Child equation

$$I = G \cdot V^{\frac{3}{2}}, \qquad V > 0, \tag{2}$$

with perveance G, a constant that only depends on the geometrical construction of the tube.

2.1.3. Saturation Current

Beyond a certain voltage, all emitted electrons are drawn to the anode. Saturation appears, that means, the current remains nearly constant when the external voltage is increased further.

2.2. Triode Characteristics

Triodes have a third electrode placed between anode and cathode, which is constructed as a wire mesh and therefor called *grid* (G). A voltage applied to the grid is able to control the flow of electrons from the cathode: a negative grid voltage causes an electric field that counteracts with the electric field from the anode, the cathode current is reduced. A higher negative grid voltage inhibits the current flow thoroughly. Small changes in grid voltage cause high changes in current flow, thus it is possible to use triodes for amplification.

For clarity we define the following conventions: V_a is the anode- and V_g the grid voltage (both referred to the cathode potential), I_k, I_a and I_g are the cathode, anode and grid currents, respectively. We define $I_g + I_a = I_k$ where I_a and I_g are directed into the device.

For the introduction of a grid between anode and cathode it is a common prospect to replace the three-terminal triode by a two-terminal one [2], where the electrode is placed at the grids' position and loaded with the *effective voltage*,

$$V_{\text{eff}} = \left(V_g + \frac{1}{\mu} V_a \right). \tag{3}$$

The amplification factor μ states about how much higher the anode current is influenced by the grid than by the anode voltage. The current I_k is calculated analog to equation (2),

$$I_k = G \cdot (V_{\text{eff}})^{\frac{3}{2}}, \qquad V_{\text{eff}} > 0. \tag{4}$$

Equation (4) is valid for the "normal" operating condition, where the grid is slightly more negative than the cathode, while the anode potential is very high (e.g. $V_g = -2\,\text{V}$ and $V_a = 300\,\text{V}$). As for the diode we speak of the *space-charge region*. The grid draws no current ($I_g = 0$) and consequentially anode and cathode current are equal, $I_a = I_k$.

As a special case we consider the operation with a positive grid. Since the grid now likewise attracts electrons, a positive current I_g arises and hence the cathode current divides into anode and grid current. Most books do not respect this case in detail, because the flow of grid current introduces distortions and thus do not satisfy the classical amplifier theory anymore. The positive grid is irrelevant for the design of linear hi-fi tube amplifiers. Fact is, that most guitar amplifier designs since the 1960s are operated under these conditions and that the grid current is responsible for some distortion effects like the *blocking distortion* [6, 7]. For a correct simulation the inclusion of the grid current can play an important role, especially if coupled stages in a cascade are examined.

3. PRACTICAL TUBES

Real tubes depart occasionally clearly from the idealized formulations given in Section 2 as well as from the information found in the manufacturer's data sheets. Aging effects, small constructive variations and origin have influence on the characteristics, to name a few reasons. Even tubes from the same type and same manufacturer may show up to 20 % deviation of each other. Exemplary measurement results are discussed e.g. in [8, 9].

3.1. Measurements

To have reliable reference data, numerous measurements on standard triodes of type 12AX7 were performed by the authors. Grid and anode current were measured at the same time in good resolution for a fine mesh of discrete V_g and V_a voltages. Since tube circuits are normally operated with AC, the measurements were not performed under static conditions, but using switched voltage supplies and triggered meters. The two DC supplies for V_a and V_g were switched on at the same time and the currents were measured for a short time period. From the stored current values the median was chosen to be the final value. The distance between the discrete measurement points was chosen small enough, that a subsequent interpolation is not required. In consideration of the constrains given by maximum power consumption and maximum anode current, the observed working range was $V_a = 20\,\text{V}$ to $300\,\text{V}$ and $V_g = -5\,\text{V}$ to $3\,\text{V}$. The discrete steps for the grid were $\Delta V_g = 0.1\,\text{V}, |V_g| < 1\,\text{V}$ and less dense for higher values, and $\Delta V_a = 20\,\text{V}$ for the anode voltage. This manually performed procedure is highly time-consuming (ca. 8h net./system), so only three triode systems were tested as a start.

At first we settle for evaluating the measurements only qualitatively, some complete datasets will be shown in Section 5.5.

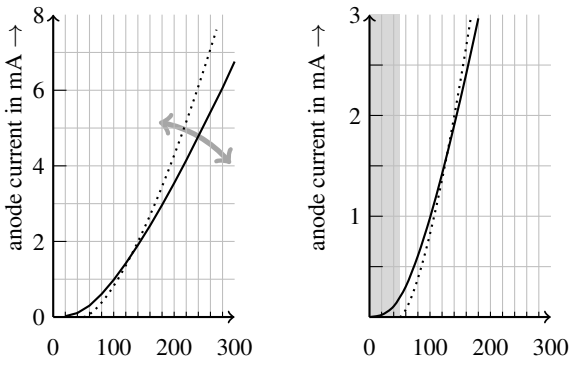

(a) *exponent variation* (b) $V_{\text{eff}} < 0$ *range*

Figure 1: *Anode current calculated with Langmuir-Childs formula (dotted) and measurements from a RSD 12AX7 triode (solid) in a qualitative plot.*

3.2. Observations on the Anode Current

Figure 1 opposes qualitatively a measurement from an old 12AX7 tube (RSD) and Langmuir-Child's law. While the measurement in principle follows the formula, two differences are visible: First, the theoretic $\frac{3}{2}$-exponent does not fit perfectly for real triodes, see 1(a). In the plotted example, the slope of the measured curve is lower, representing an exponent $< \frac{3}{2}$.

The second difference can be found at the bottom of the curve. Equation (4) yields $I_k = 0$ for $V_{\text{eff}} = 0$, and is not defined for voltages $V_{\text{eff}} < 0$. The measurement offers a small current for this case and a smooth transition towards zero current. This is depicted in Figure 1(b), where the highlighted region tags the range $V_{\text{eff}} < 0$. We will resume these points later on in Section 5.

3.3. Observations on the Grid Current

The measured grid current increases when moving from small negative voltages towards the ordinate following an exponential shape,

see Figure 2(a). For positive voltages the current increases less steep, but may reach significant values (Figure 2(b)). The grid current I_g is highly influenced by V_g, but has only small dependency on V_a.

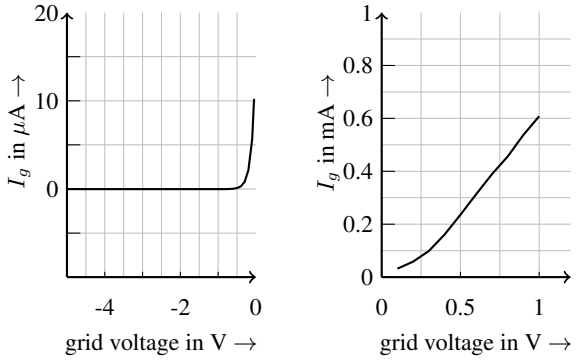

(a) *grid negative* (b) *grid positive*

Figure 2: *Grid current measured for 12AX7 triode (same tube).*

4. MODELING OF TUBES

In the last 20 years about a dozen different tube models for SPICE simulation tools were invented. These mathematical expressions are also widely used in digital audio effect algorithms. For application of those SPICE models we refer to a recent book [9] and the original papers.

Basically we can distinguish between *physical* models, which are based on the physical tube equations and *heuristic* or *phenomenological* models, which have no physical foundation. A different distinction can be made by classifying models by purpose of use. While the first tube models were motivated by SPICE-based hi-fi circuit analysis, the newer models are explicitly invented for guitar amplifier simulation. In the following we will review three approaches briefly to get an introduction to the subject.

One of the most popular models is a phenomenological description invented by Koren [10]. In his approach the triode is composed from basic SPICE components, namely current sources, resistors and diodes and a mathematical description. The work features a library with popular tubes. Koren's model gives good results for simulations with negative grid.

A recent model was proposed by Cardarilli *et al.* [11]. In their formulation the "tube constants" (e.g. μ, G) are exchanged by 3rd-order polynomials, then the model (with its many unknowns) is fitted to measurement data. The presented results, including the simulation of a guitar amplifier, are very promising. Nevertheless the formula has lack of physical interpretation, because the polynomial for the perveance, which is the only real constant, has a high excursion.

Cohen and Helie [12] extended Koren's model by a more realistic grid current, using a piecewise-defined function with a linear part, a second-order polynomial and a smooth transition. They performed current measurements in a similar manner, followed by a bilinear interpolation. Based on these data a fitting is executed, identifying Koren's parameters individually for three triodes.

5. NEW TRIODE MODEL

Based on the observations from Section 3 a new triode desription is deployed. We follow the idea, that the model in general has to be physically motivated, i.e. the formulations have to follow the traditional equations as explained in the second section. Furthermore the model has to be adaptable, so that simulations can be fitted individually to a selected tube. Last but not least, formulations with low complexity are desirable, to enable real-time applications.

5.1. Cathode Current

The exponent in equation (4) may differ from the theoretical value $\frac{3}{2}$, as already stated in Section 3.2. This can be explained by the fact, that the exponent is calculated for simplified and ideally constructed triodes and thus may differ from practical ones.

Kniekamp focused in a historic study on the exponent and specified several counteracting reasons for the deviation [13], saying that the exponent may be both smaller or greater than 1.5. Reich [1] identified the exponent generously to be approximately in the range 1.2 to 2.5.

In fact, this was already part of other triode models, Koren for example assumed a fixed exponent of 1.4 in his model [10]. In the upcoming model the exponent will be parametrized with γ. This leads to the first approximation for the cathode current

$$I_k \approx G \cdot (V_{\text{eff}})^{\gamma}, \qquad V_{\text{eff}} > 0. \tag{5}$$

Note that the transition for $V_{\text{eff}} \leq 0$ is not considered in this equation.

5.2. Grid Current

With a view to the mechanical construction it is obvious that the relation between grid and cathode can be modeled roughly as a vacuum diode. The variables may differ considerably since the grid electrodes' construction is distinct from the solid anode. But in general any N-electrode arrangement will show an initial velocity current and space-charge effects, cf. [2].

From the measurements we found, that the grid current I_g is highly influenced by the grid voltage, but has only small dependency on the anode voltage. This leads to a simplified approximation for $I_g = f(V_g)$,

$$I_g \approx G_g \cdot V_g^{\xi} \tag{6}$$

with the grid perveance G_g and exponent ξ. Similar observations are specified in [12] and supported by the literature [2, 4]. Note that equation (6) corresponds to the space-charge law, equation (4), but with possibly deviant exponent. Near to $V_g \approx -0$ the grid current was measured to resemble an exponential curve. This can be explained by the initial velocity current, as in equation (1).

5.3. Smooth Transition

To create a smooth transition between piecewise functions various approaches are possible. For our model we decided to use a combination of exponential function and logarithm. As introduction we examine a simple function $f(x)$ with

$$f(x) = \begin{cases} x & , x > 0 \\ 0 & , x < 0. \end{cases} \tag{7}$$

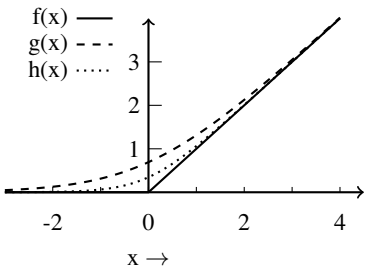

Figure 3: *Smoothing function.*

Obviously there is a knee at $x = 0$. To smoothen this discontinuity we consider a second function

$$g(x) = \log(1 + e^x) \tag{8}$$

showing the same tendencies as equation (7) for greater values of $|x|$. With increasing x the result tends to $g(x) \approx \log(e^x) = x$, while the exponential and thus the function value approaches zero in $-x$ direction.

The curve shape can furthermore be adapted towards the linear function using an additional factor C, leading to

$$h(x) = \log(1 + e^{C \cdot x}) \cdot \tfrac{1}{C}. \tag{9}$$

This relation is illustrated in Figure 3, where equations (7), (8) and (9) are plotted (adaption factor was chosen $C = 2$).

With this mathematical trick the smoothing of our modeling equations comes to mind. The idea is not new, by taking a closer look to Koren's model, we figure out equation (8) in the expression for the anode current. Evidently equation (9) with the extension is more flexible.

5.4. Final Equations

The derivations for the cathode and the grid current are now assembled and the smoothing is applied to our formulations for I_k and I_g. Enhancing equation (5) and equation (6) yield the final formulations:

$$I_k = G \cdot \left(\log\left(1 + \exp\left(C \cdot \left(\tfrac{1}{\mu} \cdot V_a + V_g\right)\right)\right) \cdot \frac{1}{C} \right)^{\gamma} \tag{10}$$

$$I_g = G_g \cdot \left(\log\left(1 + \exp\left(C_g \cdot V_g\right)\right) \cdot \frac{1}{C_g} \right)^{\xi} + I_{g0}, \tag{11}$$

with the perveances G and G_g, exponents γ and ξ and the adaption factors C and C_g. For the grid current a constant I_{g0} is added due to stability reasons. The anode current subsequently has to be the difference of both, giving

$$I_a = I_k - I_g. \tag{12}$$

These equations still reveal the well-known physics but with some degree of freedom. Furthermore, they are continuously differentiable and have no discontinuities.

5.5. Fitting to the Measurements

The model equations feature four free parameters for the cathode current (G, C, μ, γ) and four for the grid current (G_g, C_g, ξ, I_{g0}).

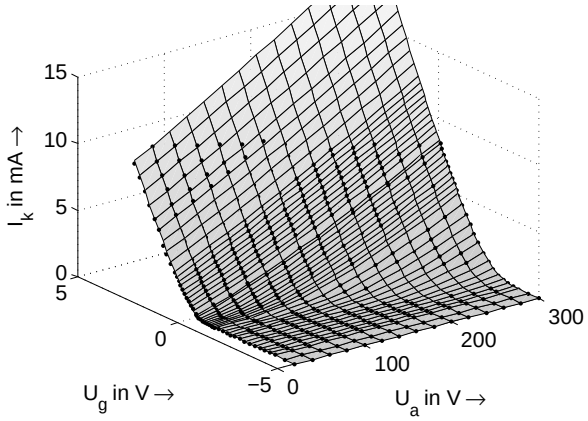

Figure 4: *Fitting of equation* (10) *to measured* I_k.

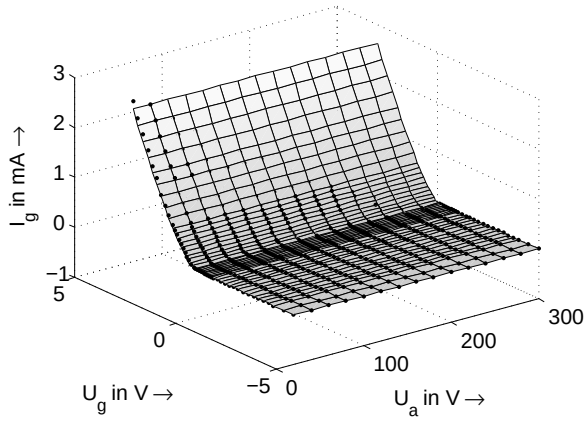

Figure 5: *Fitting equation* (11) *to measured* I_g.

Using a curve fitting algorithm like `sftool`[1] it is now possible to adapt the parameters to the measurement data. Figure 4 shows both measurement data and fitting curve of the cathode current for a 12AX7 triode, displayed as a 3-D plot. The surface represents the analytically computed characteristics according to equation (10) while the measurements are given as black dots. The influence of the grid voltage on the current is obvious. Figure 5 displays the same for the grid current, revealing that I_g is almost independent of V_a, as mentioned before. It can be asserted that the measurement dots align well with the surfaces for both plots.

The fitting results for three systems are given in Table 1. Fortunately, G, μ and γ reflect the standard values that can be found in the books in a satisfying approximation.

The 3-D plots are nice for getting an idea of the dependencies, although parametric curves allow for a better inspection of the results. In Figure 6 the complete characteristics of a measured triode are compared to the results from the fitting. The influence of grid and anode voltage on the currents is clearly visible and accurately replicated by the model.

[1] Surface Fitting Toolbox for MATLAB, The Mathworks

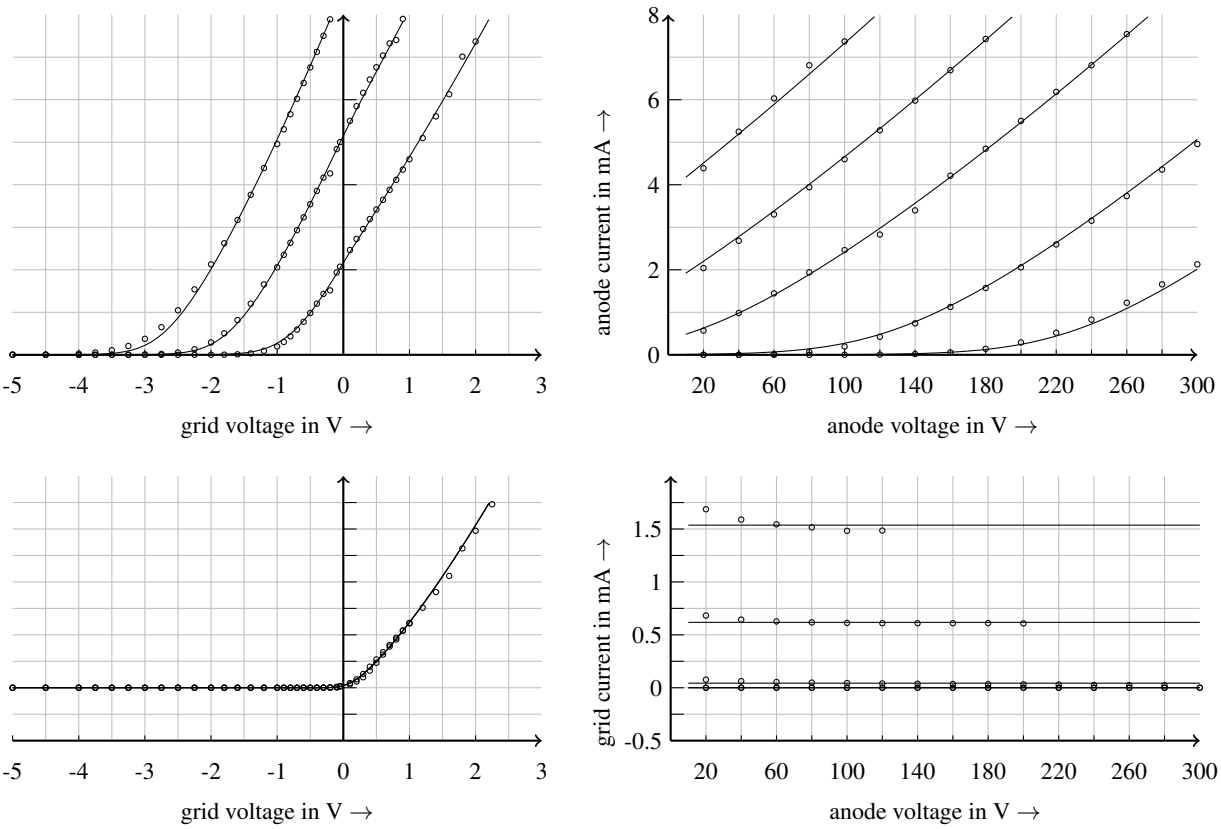

Figure 6: *Complete characteristics of a 12AX7 triode. In black: simulation results, ∘: measurement data from a RSD tube. Plots on the left: grid family for V_a =*100 V, 200 V *and* 300 V. *Plots on the right: plate family for V_g =*−2 V, −1 V, 0.1 V, 1 V *and* 2 V.

	RSD-1	RSD-2	EHX-1
G	2.242E-3	2.173E-3	1.371E-3
μ	103.2	100.2	86.9
γ	1.26	1.28	1.349
C	3.40	3.19	4.56
G_g	6.177E-4	5.911E-4	3.263E-4
ξ	1.314	1.358	1.156
C_g	9.901	11.76	11.99
I_{g0}	8.025E-8	4.527E-8	3.917 E-8

Table 1: *Individually fitted parameters for 12AX7 triodes.*

5.6. Parasitic Capacitances

The electrodes and their mechanical assembly lead to parasitic capacitances which have to be taken into account for a correct dynamic behavior. As in other existing tube models we assume the standard values that can be found in the data sheets, i.e. $C_{ak} = 0.9\,\text{pF}$, $C_{gk} = 2.3\,\text{pF}$ and $C_{ag} = 2.4\,\text{pF}$ for 12AX7.

6. RESULTS

6.1. Comparison with other Models

The proposed model has to be compared to the existing approaches. Figure 7 shows again the family characteristics of the new model (black curves) and the measurements of one tube (circles). The dotted curves show the characteristics of Koren's model [10]. The curves have generally the same progression. Differences are found for the grid current (lower plots) and for the shape of the anode current for positive grid voltages.

This observation is not surprising. The new model was individually fitted to the measurement data, so the black curves should align better with the circles than the general Koren model. More meaningful is the comparison to other individual models. We decided to examine the individual model proposed by Cohen and Helie [12]. It is based on Koren's formula, but with a different grid current where a piecewise-defined function with three subdomains is suggested. To achieve an equitable comparison the equations were fitted in a similar manner to the same measurement data. The results are displayed in Figure 7 as dashed curves. The improvement due to the individualization is clearly visible and the curves align better with the measurements.

Regarding our approach a deviation remains for high anode voltages and negative grid voltage (see upper left plot), where the standard Koren model interestingly performs best. Besides, the shape for very low anode voltages ($V_a < 20\,\text{V}$) is not captured correctly.

However, in this comparison the proposed equations allowed better fitting results and achieved a good alignment with the measurements. The same observation was made for the other tested triodes.

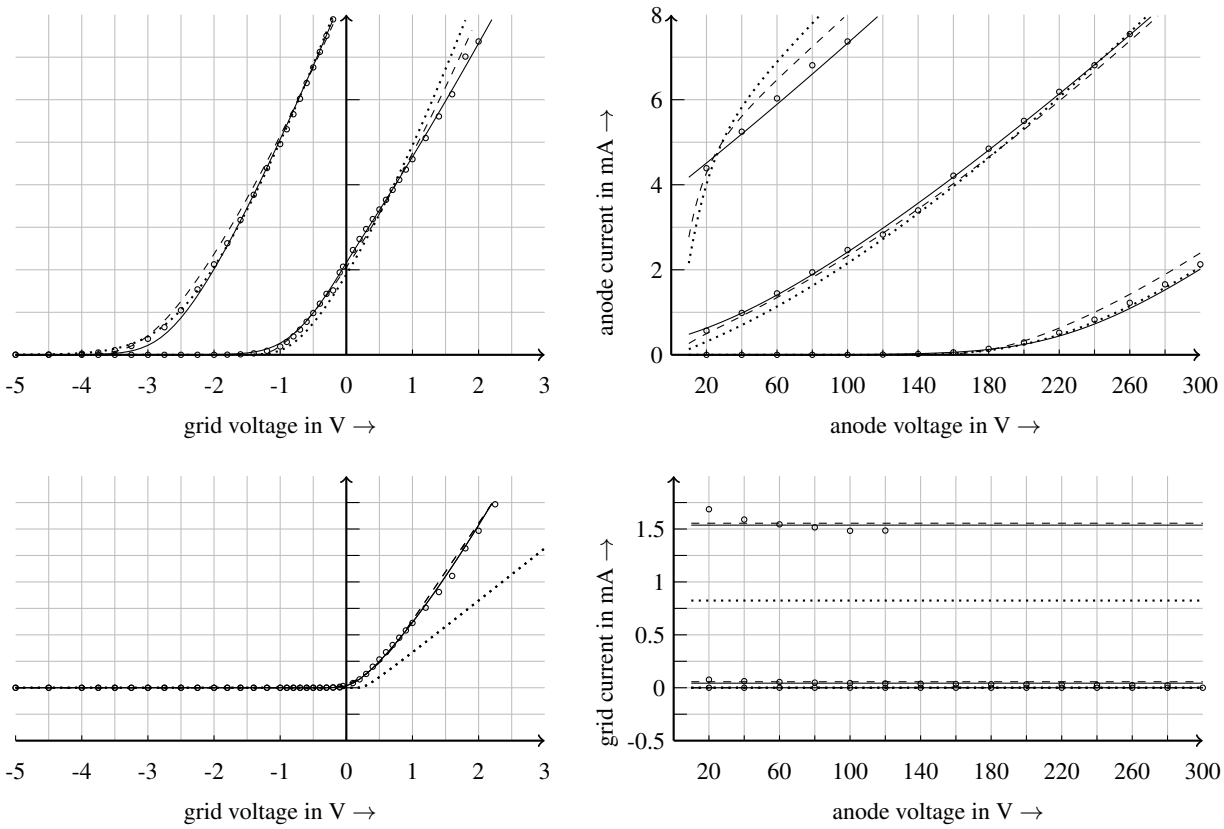

Figure 7: *Comparison of different triode models. Plots on the left: grid family for V_a =100 V and 300 V. Plots on the right: plate family characteristics for V_a =−2 V, 0.1 V and 2 V. Shown are Koren's approach (dotted), Cohen and Helie (dashed) and the new model (black). The discrete measurement points are marked with ∘.*

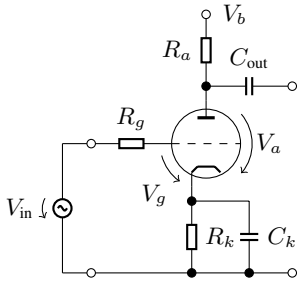

Figure 8: *Common-cathode amplifier stage.*

6.2. Application: Common-Cathode Amplifier Stage

To check to what extent the model equations replicate real triodes when used within a circuit simulation, a common tube amplifier stage was prototyped. The same tubes as those used in the fitting procedure were operated in this test circuit and the responses to various excitation signals were measured.

Figure 8 depicts the schematic of the chosen amplifier stage. This common-cathode amplifier can be found in almost all preamplifiers designs. We skip a detailed circuit analysis and are content with the information, that this represents an inverting amplifier giving a high gain. The operating point is a bit negative, but for higher input amplitudes the grid will be temporarily positive. Several papers analyzed this simple but representative circuit and discussed qualified simulation techniques [9, 12, 14, 15].

For the simulation of the circuit a state-space model was implemented. The state-space representation has turned out to be a practical tool for the simulation of nonlinear circuits [16]. We skip the details of the implementation and refer to a recent study dealing with this method [17]. The state-space representation gets along with four state variables, two for the shown capacitors C_{out} and C_k and two for the parasitic capacitances of the triode. In fact, in Section 5.6 we introduced three capacitances (C_{ak}, C_{gk} and C_{ag}) but they are not independent and thus can be reduced to two.

6.2.1. Waveforms

A comparison of time signals is given in Figure 9, where the similarity for different frequencies and input amplitudes is checked. As expected, the waveforms for higher input amplitudes are distorted. The measured and simulated outputs align well and only small differences can be observed. All measurements and simulations were performed with a sampling frequency $f_s = 96\,\text{kHz}$.

6.2.2. Harmonic Spectra

Waveform comparisons give only limited information on how good a simulation performs. In addition, the harmonic content of the

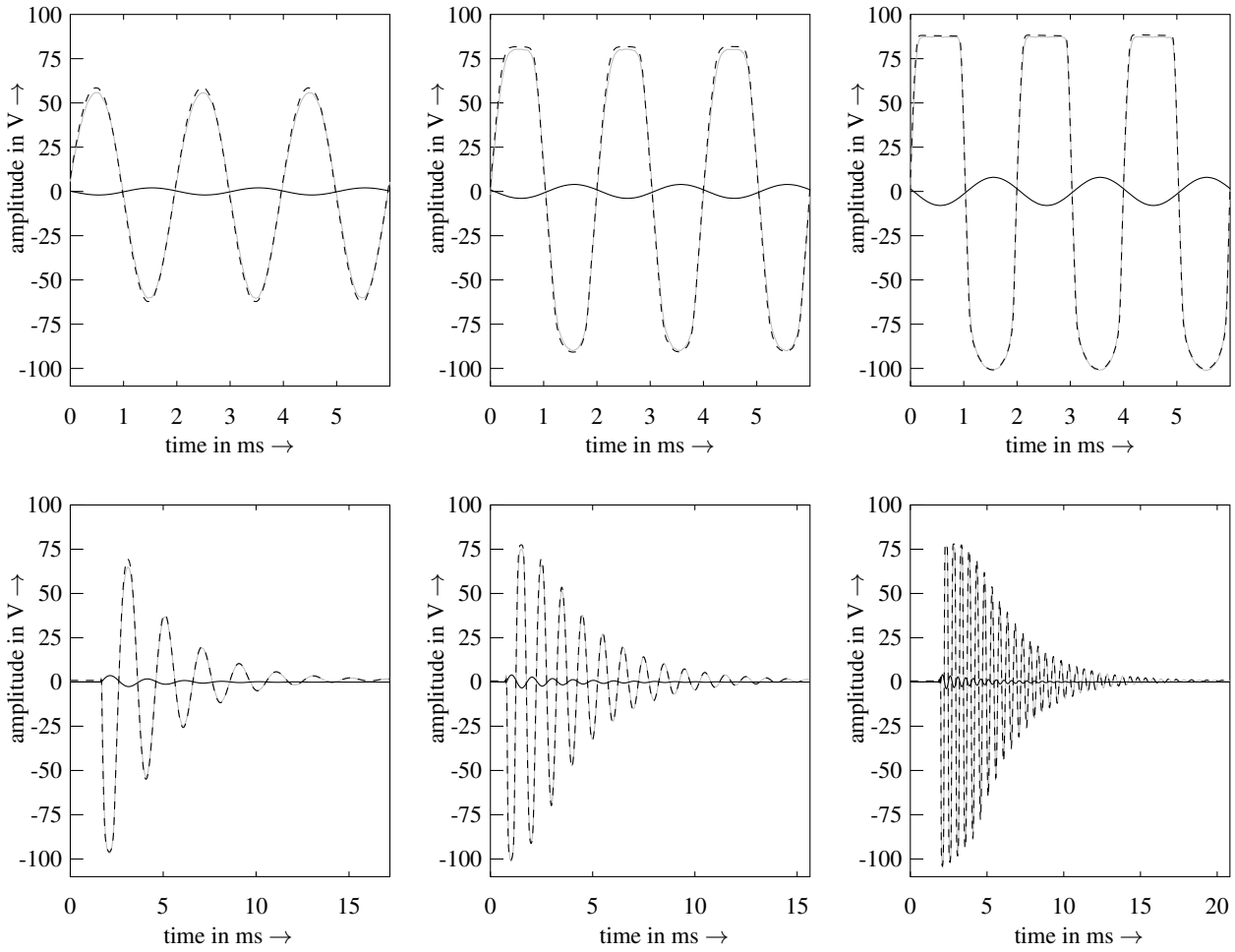

Figure 9: *Waveform comparison of measurement (gray) and simulation (dashed black) for different input signals (solid black). First row: sinusoidal excitation with* 500 Hz *and* 2 V, 4 V *and* 8 V. *Second row:* 4 V *sine burst for frequencies* 500 Hz, 1 kHz *and* 2 kHz.

output is computed both for reference system and simulation. The exponential sweep technique [18] was used to measure the introduced distortion. Figure 10(a) shows the harmonic distortions of the discussed circuit for a 4 V measurement signal. The results of the simulation are given in 10(b). As the plots illustrate, a satisfying similarity is achieved. Differences are visible at high frequencies, where the simulation is a bit flatter.

6.2.3. Guitar Sound

Some sound clips of electric guitar playing are recorded with the circuit and simulated. The comparison supports the good conformance of the results. The clips are available on our homepage `http://ant.hsu-hh.de/dafx2011/tubemodel`

6.3. Limitations

The measured type of triode 12AX7 is known as a *linear* tube [9]. Keeping guitar amplifier distortion in mind this may confuse at first. But the classification linear or nonlinear regime depends on the course of the amplification factor μ. A typical example for a nonlinear triode is the 12AT7, which can be found in audio circuits (e.g. phase inverter stages) as well. In addition to the 12AX7 measurements, one 12AT7 triode was checked. It was found that the fitting results are not as good as for the 12AX7 tubes. Especially the assumption that I_g is almost independent of V_a is not valid anymore. As a second limitation we have to respect a lower bound for the anode voltage. When operating the triode model in the region with $V_g > 0$ and small anode voltages, say $V_a < 20\,\mathrm{V}$, the results are obviously not correct. For real triodes the anode current will decrease rapidly when approaching $V_a = +0\,\mathrm{V}$, an effect that is not reproduced by the presented formulations.

7. DISCUSSION AND OUTLOOK

The proposed equations are able to characterize the behavior of real triodes in a good accordance. One advantage over other descriptions is that the equations can be educed from the fundamental laws to a large extent.

Though there are some restrictions as identified by the comparisons. As already stated, the shape for very low anode voltages ($V_a < 20\,\mathrm{V}$) is not captured correctly. But normally the 12AX7

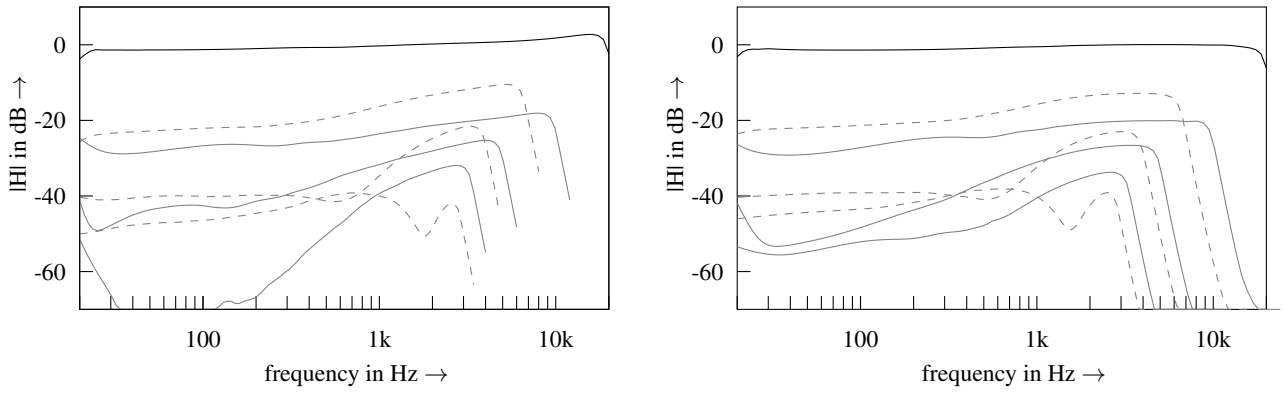

(a) *measurement* (b) *simulation.*

Figure 10: *Frequency domain analysis of the common-cathode amplifier. Smoothed harmonic spectra for a sweep with* 4 V *amplitude. Shown are the fundamental (black), odd (dashed gray) and even order harmonic responses (solid gray).*

triode will not be operated in this region, because the internal resistance approaches a finite value for all anode voltages. Hence this shortcoming is considered to be marginal.

As a future prospect more tubes have to be inspected with even higher resolution of the discrete measurement points to improve the quality of the fittings. Furthermore the model has to enhanced so that nonlinear triodes are comprised, too.

8. CONCLUSION

A new model for triodes of type 12AX7 was presented, featuring a good replication of the grid current and physically-motivated formulations. The equations are mainly based on the Langmuir-Child's law and can be calculated separately for cathode and grid current.

Free parameters within the formulations were used to perform an individual fitting to measurement data of practical triodes. It was shown, that the equations are able to characterize the properties of real tubes in good accordance.

To prove the suitability for the simulation of audio circuits, the model was embedded in a state-space description of a typical tube preamplifier. The simulation results for different input amplitudes and frequencies were compared to reference measurements and showed a good match. The derived equations are simple, continuously differentiable and applicable for real-time simulations.

9. REFERENCES

[1] H. Reich, *Principles of Electron Tubes*, McGraw Hill, 1st edition, 1941.

[2] H. Barkhausen, *Lehrbuch der Elektronenröhren und ihrer technischen Anwendungen*, Verlag S. Hirzel, Leipzig, 1945.

[3] K. Spangenberg, *Vacuum Tubes*, McGraw Hill, 1942.

[4] H. Rothe and W. Kleen, *Grundlagen und Kennlinien der Elektronenröhren*, Geest & Portig, Leipzig, 1951.

[5] J. Pakarinen and D. T. Yeh, "A review of digital techniques for modeling vacuum-tube guitar amplifiers," *Computer Music Journal*, vol. 33, no. 2, pp. 85–100, Summer 2009.

[6] M. Blencowe, *Designing Tube Preamps for Guitar and Bass*, Blencowe, 2009.

[7] R. Aiken, "What is blocking distortion?," [online], www.aikenamps.com/BlockingDistortion.html, 1999.

[8] M. Zollner, *Physik der Elektrogitarre*, (preprint), Regensburg, 2010.

[9] A. Potchinkov, *Simulation von Röhrenverstärkern mit SPICE*, Vieweg + Teubner, 1st edition, 2009.

[10] N. Koren, "Improved vt models for spice simulations," *Glass Audio*, vol. 5, pp. 18–27, 1996.

[11] G. C. Cardarilli, M. Re, and L. Di Carlo, "Improved large-signal model for vacuum triodes," in *IEEE International Symposium on Circuits and Systems (ISCAS)*, 2009, pp. 3006–3009.

[12] I. Cohen and T. Helie, "Measures and parameter estimation of triodes, for the real-time simulation of a multi-stage guitar preamplifier," in *Proc. 129th AES Convention*, San Francisco, USA, Nov 4-7 2010, number 8219.

[13] H. Kniekamp, "Die Abweichungen der Verstärkerröhrenkennlinien vom $e^{3/2}$-Gesetz," *Telegraphen- und Fernsprechtechnik*, vol. 20, no. 3, pp. 71–76, 1931.

[14] J. Macak and J. Schimmel, "Real-time guitar tube amplifier simulation using an approximation of differential equations," in *Proc. of the 13th Int. Conference on Digital Audio Effects (DAFx-10)*, Graz, Austria, Sept. 6-10 2010.

[15] F. Santagata, A. Sarti, and S. Tubaro, "Non-linear digital implementation of a parametric analog tube ground cathode amplifier," in *Proc. of the 10th Int. Conference on Digital Audio Effects (DAFx-07)*, Bordeaux, France, Sept. 10-15 2007.

[16] D.T. Yeh, *Digital Implementation of Musical Distortion Circuits by Analysis and Simulation*, Ph.D. dissertation, Stanford University, June 2009.

[17] K. Dempwolf, M. Holters, and U. Zölzer, "Discretization of parametric analog circuits for real-time simulations," in *Proc. of the 13th Int. Conference on Digital Audio Effects (DAFx-10)*, Graz, Austria, Sept. 6-10 2010.

[18] A. Farina, "Simultaneous measurement of impulse response and distortion with a swept-sine technique," in *108th AES Convention*, Paris, France, Feb. 19-24 2000.